Materials Science Forum
ISSN: 1662-9752, Vol. 1062, pp 298-303
doi:10.4028/p-n0z51t

Submitted: 2021-10-15
Revised: 2022-03-16
Accepted: 2022-03-17
Online: 2022-05-31

Microscopic Evaluation of Al_2O_3/p-Type Diamond (111) Interfaces Using Scanning Nonlinear Dielectric Microscopy

Yu Ogata[1,a*], Kohei Yamasue[1,b], Xufang Zhang[2,c], Tsubasa Matsumoto[2,d], Norio Tokuda[2,e] and Yasuo Cho[1,f]

[1]Tohoku University, 2-1-1 Katahira, Aoba, Sendai, Miyagi 980-8577, Japan

[2]Kanazawa University, Kakumamachi, Kanazawa, Ishikawa 920-1192, Japan

[a]ogty1998@riec.tohoku.ac.jp, [b]yamasue@riec.tohoku.ac.jp, [c]zhang-xufang@se.kanazawa-u.ac.jp, [d]t-matsumoto@se.kanazawa-u.ac.jp, [e]tokuda@ec.t.kanazawa-u.ac.jp, [f]yasuocho@riec.tohoku.ac.jp

Keywords: diamond semiconductor, scanning nonlinear dielectric microscopy

Abstract. Improvement of channel mobility is required to improve the performance of the inversion channel MOSFETs using diamond. The previous studies have suggested that high interface defect density (D_{it}) at the Al_2O_3/diamond (111) interface has a significant impact on the carrier transport property on a channel region. To investigate the physical origins of the high D_{it}, especially from microscopic point of view, here we investigate Al_2O_3/p-type diamond (111) interfaces using scanning nonlinear dielectric microscopy (SNDM). We find the high spatial fluctuations of Al_2O_3/hydroxyl (OH)-terminated diamond (111) interface properties and their difference by the flatness of the diamond surface.

Introduction

Because diamond possesses a high breakdown electric field, high thermal conductivity, and high carrier mobility, it has a potential to realize the power devices with high breakdown voltage, high power, and high-speed operation [1-3]. Recently, inversion type p-channel MOSFETs with normally off characteristics have been fabricated using a P-doped and OH-terminated diamond body on a diamond (111) substrate with an atomic layer deposited (ALD) Al_2O_3 dielectric [4]. In addition to the ALD Al_2O_3 dielectric, OH-termination of the diamond surface is a key for fabricating normally-off and inversion type MOSFETs suitable for power device applications and has been applicable to a (111) surface rather than (100) surface often used for diamond devices [5, 6]. However, the device performance of these MOSFETs is still unsatisfactory. In particular, the improvement of the channel mobility is one of the major issues towards the practical application of the diamond based power devices [4, 5]. In this regard, the previous studies have suggested that high interface defect density (D_{it}) at the Al_2O_3/diamond (111) interface significantly reduced the channel mobility in the MOSFETs [7]. In order to give microscopic insights on the physical origin of the high D_{it}, here we investigate the Al_2O_3/p-type diamond (111) interfaces using scanning nonlinear dielectric microscopy (SNDM) [8]. In this paper, we investigate the Al_2O_3/p-type diamond (111) interfaces by differential capacitance (dC/dV) imaging by the conventional SNDM, local capacitance-voltage (CV) profiling, and local deep level transient spectroscopy (DLTS) based on a recently developed time-resolved SNDM setup [9].

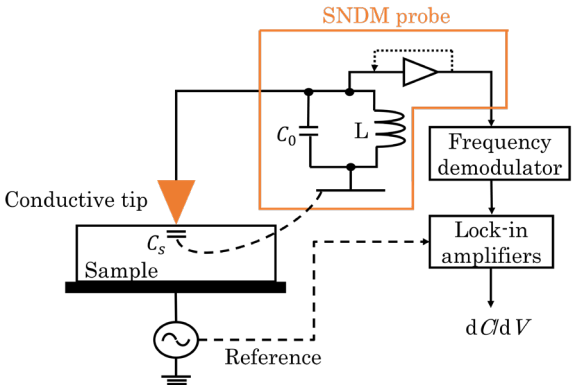

Fig. 1 Schematic diagram of SNDM

Methods

d*C*/d*V* imaging by conventional SNDM. Figure 1 shows a schematic diagram of the conventional SNDM [8]. By applying a small sinusoidal voltage to the sample and using a lock-in amplifier, we can obtain the voltage derivative of the capacitance, or d*C*/d*V*. The d*C*/d*V* images reflect the spatial fluctuations of the semiconductor properties such as the polarity of majority carriers, their density distribution, D_{it}, and density of the fixed charge in the insulating layer, due to their impacts on the local CV profile. Therefore, these semiconductor properties can be evaluated at the nanoscale by d*C*/d*V* imaging. In the time-resolved SNDM, the output signal of the SNDM probe is digitized directly and then the shift of the oscillation frequency is numerically demodulated by offline signal processing [9]. Compared to the conventional SNDM, much wider measurement bandwidth becomes possible and offline digital processing techniques permits the demodulation of capacitance variation without significant signal distortion.

Local CV profiling and DLTS. Local CV profiles can be obtained corresponding to the linear voltage changes of the triangular pulse when we apply a large amplitude triangular voltage pulse to the sample [10]. From the data, we can also extract d*C*/d*V* images by mapping the slopes of the profiles at a particular voltage. Local CV profiling can give insights on microscopic real-space fluctuations of interfacial properties. Note that our method basically reflects local CV profiles at deeply depleted high-frequency rather than low-frequency counterparts. This is because our local CV profiling uses a voltage sweep rate typically as high as several tens of kilohertz, which is much higher than standard macroscopic quasi-static CV profiling and does not allow the generation of an inversion layer.

Macroscopic DLTS is a method of analyzing defects in semiconductors proposed by Lang in 1974 and can evaluate D_{it} as well [11]. Time-resolved SNDM can be used to perform a microscopic DLTS called local DLTS. In the local DLTS, a rectangular voltage pulse is applied to the sample as in the macroscopic DLTS. We demodulate local transient capacitance response on each measurement point and, by analyzing it, we obtain the microscopic distribution of D_{it}. It has been reported that the spatial resolution of local DLTS is about the tip diameter under typical measurement conditions [12].

Results and Discussions

Samples. The samples for the SNDM measurements were prepared using process and techniques described in Refs. [5, 6, 13, 15-17].The individual samples had a Al_2O_3 insulating layer (50 nm) formed by atomic layer deposition (ALD) [5], a high-pressure high-temperature (HTHP) synthesized p-type diamond (111) substrate (2 mm×2 mm×300 μm) with a boron concentration of 10^{17} cm^{-3}, a high B concentration p+ diamond CVD layer (200 nm) for ohmic contact formation, and a vacuum deposited gold electrode layer with a thickness of 200 nm [13]. In this study, we measured three different samples, with different termination process by H, O, and OH-groups [6]. They are here denoted by H-, O-, OH-diamond (111), respectively. The diamond (111) surface with atomically flat regions was formed by anisotropic diamond etching process based on a carbon solid solution reaction into Ni [15]. Conventional plasma processes for diamond etching were not used here because of low selectivity and plasma-induced damage [15]. In addition, hydrogen plasma etching was performed to form an atomic step-terrace regions on the p-type diamond surface [16] prior to the ALD process [5]. As reported in Ref. [13], the samples without Al_2O_3 had atomically-well defined diamond (111) surface with step-terrace and bunching-step regions. SNDM measurements were performed in air at room temperature. We used a Pt-Ir coated conductive cantilever with a tip radius of 2 μm (Nanotools, C2520094). The reason for choosing such a large radius tip was to increase the signal-to-noise ratio in SNDM measurements. The voltage was applied to the sample relative to the grounded tip. SNDM was combined with a commercial scanning probe microscopy setup (Bruker, Icon) operated in contact-mode atomic force microscopy.

Results of local CV profiling. We begin with the results of local CV profiling based on time-resolved SNDM. The measurement was performed by applying a triangular voltage pulse including backward and forward sweep directions. Each sweep direction had 10 μs length. The amplitude of the pulse was

55 V_{pp} for Al_2O_3/H-diamond (111) and 70 V_{pp} for Al_2O_3/O- and OH-diamond (111). These amplitudes were chosen so that the features of the local CV profiles were obtained for each sample, taking care to avoid dielectric breakdown. The triangular voltage pulse was applied for 1000 times and resultant 1000 capacitance responses were averaged at each measurement position of 50×50 lattice points within a 5×5 μm scanned area. Figure 2 shows typical local CV profiles each selected from 2500 H-[Fig. 2(a)], O-[Fig. 2(b)], and OH-diamond (111) [Fig. 2(c)] data. The blue and red profiles in Fig. 2 show the characteristics obtained from the increasing and decreasing parts of the triangular voltage pulse, respectively. In all samples, we confirmed that local CV profiles had positive slopes resulting from p-type majority carriers. In addition, the H-diamond (111) sample showed accumulation even around 0 V, while the interfaces of the O- and OH-diamond (111) samples were depleted around 0 V. This is due to negative electron affinity of the H-diamond surface causing the high hole concentration [14].

These profiles showed different slopes in the transition from depletion to accumulation. From Fig. 2, the maximum slopes of the local CV profiles for H-, O-, and OH-diamond (111) samples were estimated to be 68 aF/V at -24 V, 10 aF/V at 11 V, and 51 aF/V at 21 V, respectively, by numerical differentiation. Since the transition occurs more rapidly and capacitance change becomes higher as D_{it} decreases, D_{it} is the lowest at the Al_2O_3/H-diamond (111), followed by Al_2O_3/OH-, and O-diamond (111) interfaces. Figure 3 shows two-dimensional maps of dC/dV at the above mentioned voltages for H-[Fig. 3(a)],O-[Fig. 3(b)], and OH-diamond (111) [Fig. 3(c)]. For all samples, the dC/dV images have non-uniform distributions.

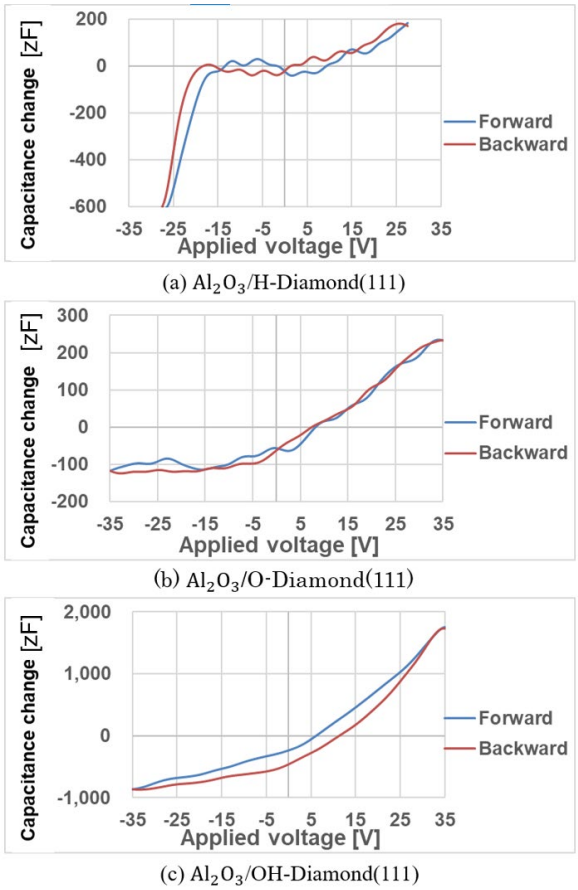

Fig. 2 Local CV profiles of the Al_2O_3/diamond (111) samples with different interface termination processes

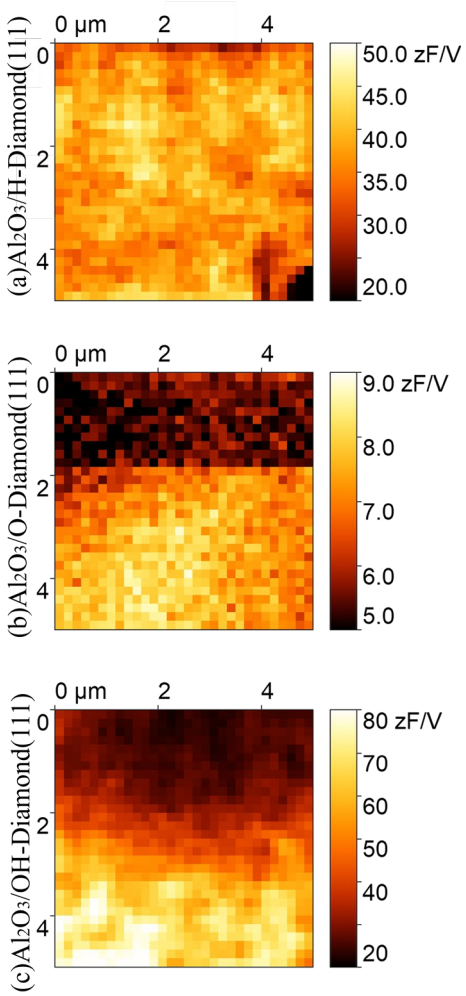

Fig. 3 dC/dV images reconstructed from local CV profiles

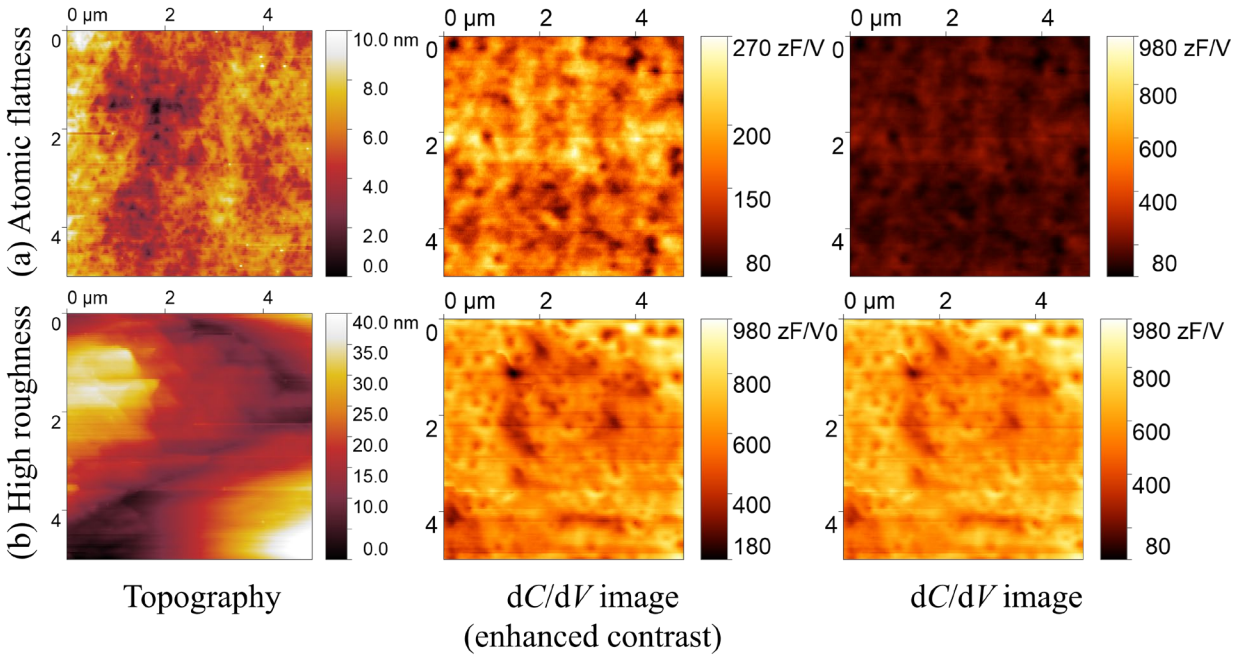

Fig. 4 Topographic and dC/dV images of the Al_2O_3/OH-diamond(111) sample with different flatness. The dC/dV images on the right have the same color-scale.

According to our recent work [17], on the H-diamond (111) sample, because the number of the dangling bonds generating D_{it} on the diamond (111) surface is equivalent to the valence of hydrogen atoms, it is considered that the dangling bonds can be drastically reduced by hydrogen termination. On the other hand, on the O-terminated sample, D_{it} is high because double bonds can also be formed between oxygen and carbon atoms, generating new dangling bonds. For the OH-diamond sample, we can expect that D_{it} is lower than that in the O-diamond sample because of matching between the valence of the OH group and a surface carbon atom. However, it is pointed out that there is a possibility that the effectiveness of the OH-termination process largely depends on the topography of a diamond surface and could leave and generate high D_{it} at the Al_2O_3/diamond interface [13]. Since the Al_2O_3/OH-diamond (111) interface is important to bring out the performance of inversion type diamond MOSFETs [5, 7, 13], we here focus on the OH-diamond (111) sample. We performed dC/dV imaging by the conventional SNDM and D_{it} imaging by local DLTS on the different areas of the OH-diamond (111) sample with different flatness.

dC/dV imaging. Figure 4 shows topography and dC/dV images of the Al_2O_3/OH-diamond (111) sample. For dC/dV imaging, we applied a sinusoidal voltage with a frequency of 30 kHz and an amplitude of 3.0 V_{pp}, together with a DC voltage of 5 V. The frequency chosen here was typically used for SNDM imaging. The amplitude and DC voltage were adjusted to obtain sufficiently high signal strength of the dC/dV signal. We obtained dC/dV images and topography at the same time with a resolution of 512×128 pixels. Figures 4(a) and 4(b) show topography and dC/dV images on an area with atomic flatness and adjacent rough area, respectively. Only the topographic images were here flatten as normally done in AFM imaging. It has been confirmed that, before depositing Al_2O_3, the former area had large (111) terraces with atomic steps on the diamond surface, while the adjacent latter area exhibited higher roughness because of insufficient planarization on the same sample, as reported in Ref. [13]. From the topographic images in Fig. 4, the roughness values after Al_2O_3 deposition were about 1 nm for the flat area and 10 nm for the rough area in root-mean-square. In Fig. 4, both dC/dV images had spatial fluctuations where dark spots possibly were non-uniformly distributed. In more detail, on the atomically flat area in Fig. 4(a), the dark spots are densely and evenly seen in the dC/dV image over the measurement area. In contrast, on the area with higher roughness in Fig. 4(b), the dark spots in the dC/dV image are concentrated on a portion of the scanned

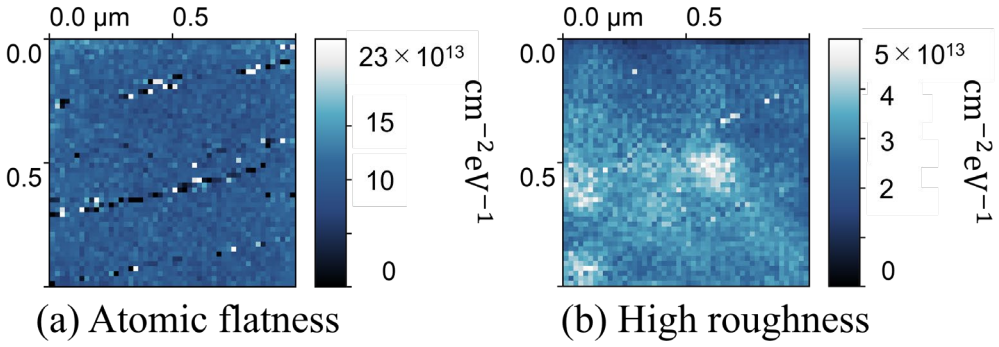

Fig. 5 Local DLTS images of Al_2O_3/OH-diamond(111) sample with different flatness

area. These dark spots possibly indicate high D_{it} regions with lower dC/dV, and the difference in their spatial distributions suggests that dC/dV images visualize the difference of the spatial D_{it} distribution in different surface flatness.

***D*it imaging by local DLTS.** In order to directly image spatial D_{it} distribution especially on the Al_2O_3/OH-diamond (111) sample, local DLTS based on time-resolved SNDM was further performed. As an accumulation pulse, 5 μs-long rectangular voltage pulse stepping down to a target level of +5 V from a reference level of -5 V was applied 1000 times and the resulting 1000 repetitive capacitance transients was averaged at each measurement position of 50×50 lattice points. The scanned area was reduced to 1 μm×1 μm for obtaining higher spatial resolution. The target and reference levels were here determined based on the local CV profiles in Fig. 2(c) to make the interface transit from depletion to accumulation. The measurement time was about 15 min. for each image. Figure 5 shows D_{it} images of the area with atomic flatness [Fig. 5(a)] and higher roughness [Fig. 5(b)]. The average of D_{it} were both as high as 10^{13} $cm^{-2}eV^{-1}$ order. Non-uniform distribution of D_{it} was observed in both images. In particular, the line-shaped features of D_{it} distribution could be observed in the atomically flat area. They might be related to the variation of D_{it} at the atomic steps in the buried interface. In fact, studies using conductive atomic force microscopy and Kelvin probe force microscopy have shown that D_{it} may differ depending on the interface step structure [13]. On the other hand, in the rough area, similar line-shaped structures could not be found in the measurement area but clustering high D_{it} regions were observed. From these results, the flattening process of the diamond surface may affect the distribution of D_{it}.

Conclusions

In this paper, SNDM based dC/dV imaging, local CV profiling, and local DLTS were carried out for the Al_2O_3/diamond (111) samples with different interface termination process. From the obtained local CV profiling, we estimated that D_{it} was the lowest in Al_2O_3/H-diamond (111), followed by Al_2O_3/OH-, and Al_2O_3/O-diamond (111) samples. For the Al_2O_3/OH-diamond (111) sample, the results of dC/dV imaging and local DLTS suggested that the flattening process of the diamond surface strongly affects the distribution and size of the interface defects.

Acknowledgments

This work was supported in part of by Grants-in-Aid for Scientific Research (S) (Grant No. 16H06360) from the Japan Society for the Promotion of Science, NEDO Uncharted Territory Challenge 2050 Grant Number 19101600-0, and Kanazawa University SAKIGAKE Project 2020.

References

[1] S. Shikata and H. Umezawa, Development of Diamond-Based Power Devices, Synthesiology English Edition 6 (2013) 147-157.

[2] C.J.H. Wort and R.S. Balmer, Diamond as an Electronic Material, Mater. Today 11 (2008) 22-28.

[3] J. Isberg, J. Hammersberg, E. Johansson, T. Wikström, D.J. Twitchen, A.J. Whitehead, S.E. Coe, and G.A. Scarsbrook, High Carrier Mobility in Single-Crystal Plasma-Deposited Diamond, Science 297 (2002) 1670-1672.

[4] T. Matsumoto, H. Kato, K. Oyama, T. Makino, M. Ogura, D. Takeuchi, T. Inokuma, N. Tokuda, and S. Yamasaki, Inversion Channel Diamond Metal-Oxide-Semiconductor Field-Effect Transistor with Normally off Characteristics, Sci. Rep. 6 (2016) 31585.

[5] X. Zhang, T. Matsumoto, S. Yamasaki, C.E. Nebel, T. Inokuma, and N. Tokuda, Inversion-Type p-Channel Diamond MOSFET Issues, J. Mater. Res. 36 (2021) 4688-4702.

[6] R. Yoshida, D. Miyata, T. Makino, S. Yamasaki, T. Matsumoto, T. Inokuma, and N. Tokuda, Formation of Atomically Flat Hydroxyl-Terminated Diamond (111) Surfaces via Water Vapor Annealing, Appl. Surf. Sci. 458 (2018) 222-225.

[7] T. Matsumoto, H. Kato, T. Makino, M. Ogura, D. Takeuchi, S. Yamasaki, T. Inokuma, and N. Tokuda, Inversion Channel Mobility and Interface State Density of Diamond MOSFET Using N-Type Body with Various Phosphorus Concentrations, Appl. Phys. Lett. 114 (2019) 242101.

[8] Y. Cho, Scanning Nonlinear Dielectric Microscopy: Investigation of Ferroelectric, Dielectric, and Semi-conductor Materials and Devices, Elsevier, ISBN9780128172469, 2020.

[9] Y. Yamagishi and Y. Cho, Nanosecond microscopy of capacitance at SiO_2/4H-SiC interfaces by time-resolved scanning nonlinear dielectric microscopy, Appl. Phys. Lett. 111 (2017) 163103.

[10] K. Suzuki, K. Yamasue, and Y. Cho, A Study on Evaluation of Interface Defect Density on High-κ/SiO_2/Si and SiO_2/Si Gate Stacks using Scanning Nonlinear Dielectric Microscopy, in 2019 IEEE International Integrated Reliability Workshop (IIRW), 2019.

[11] D.V. Lang, Deep-level Transient Spectroscopy: A New Method to Characterize Traps in Semiconductors, J. Appl. Phys. 45 (1974) 3023-3032.

[12] Y. Yamagishi and Y. Cho, High Resolution Observation of Defects at SiO_2/4H-SiC Interfaces Using Time-Resolved Scanning Nonlinear Dielectric Microscopy, Microelectron. Reliab. 88–90 (2018) 242-245.

[13] M. Nagai, R. Yoshida, T. Yamada, T. Tabakoya, C.E. Nebel, S. Yamasaki, T. Makino, T. Matsumoto, T. Inokuma, and N. Tokuda, Conductive-Probe Atomic Force Microscopy and Kelvin-Probe Force Microscopy Characterization of OH-Terminated Diamond (111) Surfaces with Step-Terrace Structures, Jpn. J. Appl. Phys. 58 (2019) SIIB08.

[14] D. Takeuchi, S. Koizumi, T. Makino, H. Kato, M. Ogura, H. Ohashi, H. Okushi, and S. Yamasaki, Negative Electron Affinity of Diamond and Its Application to High Voltage Vacuum Power Switches, Phys. Status Solidi (a) 210 (2013) 1961-1975.

[15] M. Nagai, K. Nakanishi, H. Takahashi, H. Kato, T. Makino, S. Yamasaki, T. Matsumoto, T. Inokuma, and N. Tokuda, Anisotropic Diamond Etching through Thermochemical Reaction between Ni and Diamond in High-Temperature Water Vapour, Sci. Rep. 8 (2018) 6687.

[16] H. Kuroshima, T. Makino, S. Yamasaki, T. Matsumoto, T. Inokuma, and N. Tokuda, Mechanism of Anisotropic Etching on Diamond (111) Surfaces by a Hydrogen Plasma Treatment, Appl. Surf. Sci. 422 (2017) 452-455.

[17] T. Matsumoto, X. Zhang, and N. Tokuda, Recent Progress and Issues of Diamond Metal-oxide-semiconductor (MOS) Interface for High-Frequency and Power Device Application, Vac. Surf. Sci. 64 (2021) 80-85 (In Japanese).